WATER VAPOR RETRIEVAL OVER MANY SURFACE TYPES

Christoph C. Borel, William B. Clodius and Jennifer Johnson
Astrophysics and Radiation Measurements Group, NIS-2, MS C323,
Los Alamos National Laboratory, Los Alamos, New Mexico 87545, USA
cborel@lanl.gov

ABSTRACT

In this paper we present a study of the water vapor retrieval for many natural surface types which could be valuable for multi-spectral instruments using the existing Continuum Interpolated Band Ratio (CIBR) for the 940 nm water vapor absorption feature. An atmospheric code (6S) and 562 spectra were used to compute the top of the atmosphere radiance near the 940 nm water vapor absorption feature in steps of 2.5 nm as a function of precipitable water (PW). We derive a novel technique called "Atmospheric Pre-corrected Differential Absorption" (APDA) and show that APDA performs better than the CIBR over many surface types.

1 Introduction

Two different approaches exist to retrieve columnar water vapor from imaging spectrometer data:

1. Differential absorption techniques based on:
   (a) Narrow-Wide (N/W) ratio between overlapping spectrally wide and narrow channels (Frouin et al., 1990), see left side of Fig. 1.
   (b) Continuum Interpolated Band Ratio (CIBR) between a measurement channel and the weighted sum of two reference channels, see right side of Fig. 1. (Green et al., 1989, Bruegge et al., 1990, Gao and Goetz, 1990a, and Carrére and Conel, 1993)
2. Non-linear fitting techniques which are based on spectral radiative transfer calculations (Gao and Goetz, 1990b, Green et al., 1993).

The advantage of the first approach is computational speed and of the second, improved retrieval accuracy. Our goal was to improve the accuracy of the first technique using physics based on radiative transfer. Using a modified version of the Duntley equation (Middleton, 1952, p.68) we derived an "Atmospheric Pre-corrected Differential Absorption" (APDA) technique and described an iterative scheme to retrieve water vapor on a pixel-by-pixel basis (section 2). Next we compared both, the CIBR and the APDA using the Duntley equation for MODTRAN3 computed irradiances, transmissions and path radiance (using the DISORT option). This simulation showed that the CIBR is very sensitive to reflectance effects and that the APDA performs much better (section 3). An extensive data set was created with the radiative transfer code 6S (Vermote et al., 1994) over 562 different ground reflectance spectra. The calculated relative water vapor error was reduced significantly for the APDA. In the AVIRIS case APDA technique had about 6.2% (vs. 14% for the CIBR) of the 562 spectra with a relative water

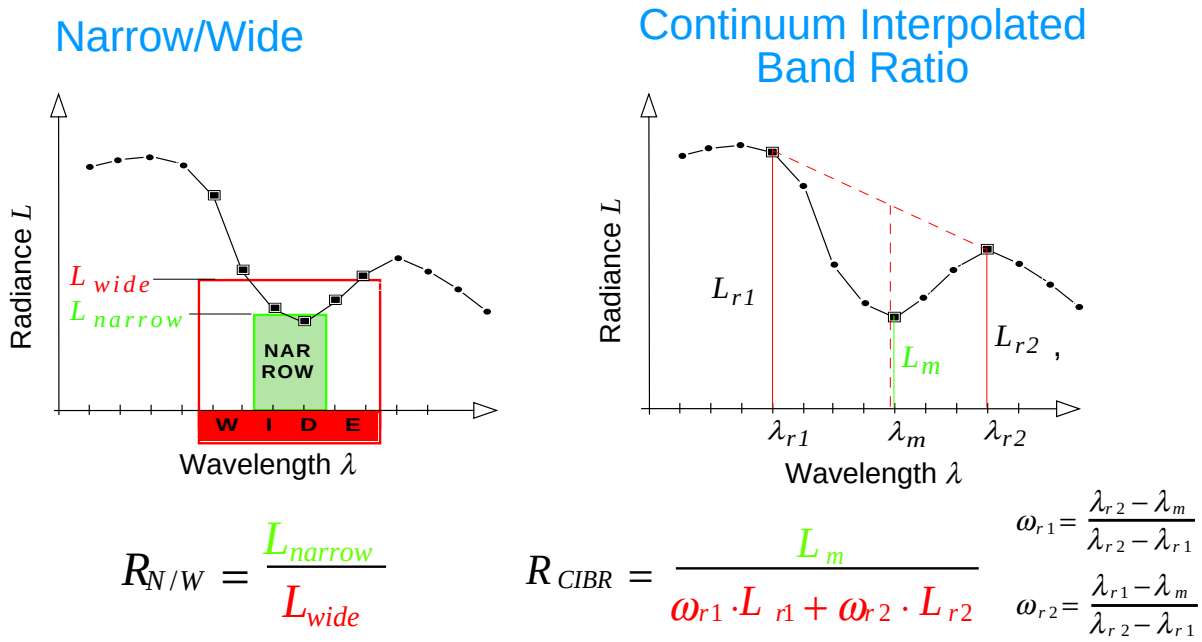

Figure 1: Narrow-Wide (NW) ratio and Continuum Interpolated Band Ratio (CIBR)

vapor error of greater than ±10% (section 4). The APDA has been applied to 1991 and 1995 AVIRIS scenes which visually demonstrate the improvement over the CIBR technique (see Schläpfer et al., 1996).

2 Derivation of the Atmospheric Pre-Corrected Differential Absorption Technique

Duntley in 1948 expressed the radiance L measured in channel i by a sensor as:

$$L_i = \rho_{g,i}\frac{E_i}{\pi}T_i + L_{h,i}(1-T_i^*) = L_{g,i}T_{0,i}T_{w,i}(PW) + L_{p,i}(PW), \quad (1)$$

where $\rho_{g,i}$ is the ground reflectance, E_i is the solar irradiance, $T_{w,i} = T_{0,i}T_{w,i}(PW)$ is the total transmission and $L_{h,i}$ is the radiance one would measure in a plane parallel atmosphere in horizontal direction and $T^*_{w,i}$ is a special transmission term (Duntley assumes: $T_{w,i} = T^*_{w,i}$). The atmospheric transmission due to water vapor PW in $[g/cm^2]$ is $T_{w,i}(PW)$. The transmission without any water vapor is $T_{0,i}$ and depends on aerosols and gas absorptions. To simplify the notation we define: $L_{g,i} = \rho_{g,i}\frac{E_i}{\pi}$. The path radiance $L_{p,i}$ is the sum of the atmospheric scattered radiance L_{atm} and the adjacency scattered radiance L_{adj}.

Using this equation we first write the radiances in three channels $i = m,\ r1$ and $r2$ where m is a measurement channel in an absorption region, e.g. the 940 nm water vapor absorption, and $r1$ and $r2$ are two reference channels. The transmission $T_{w,i}(PW)$ is a function of water vapor for channel m but not for the reference channels $r1$ and $r2$. Assuming a small difference between the central wavelengths λ_{r1} and λ_{r2} of the reference channels and $\lambda_{r1} < \lambda_m < \lambda_{r2}$ the radiance $L_m(PW)$ can be approximated by a linear interpolation as:

$$L_m = [w_{r1}L_{g,r1}T_{0,r1} + w_{r2}L_{g,r2}T_{0,r2}]T_m(PW) + L_{p,m}(PW), \quad (2)$$

where

$$w_{r1} = \frac{\lambda_{r2} - \lambda_m}{\lambda_{r2} - \lambda_{r1}} \quad \text{and} \quad w_{r2} = \frac{\lambda_m - \lambda_{r1}}{\lambda_{r2} - \lambda_{r1}}. \tag{3}$$

Note that we assume the reference channels have no water vapor absorption or $T_{r1}(PW) = 1$ and $T_{r2}(PW) = 1$. Solving equation (2) for the transmission in the water vapor channel $T_m(PW)$ and substituting $L_{g,r1}$ and $L_{g,r2}$ from equation (1) we find an equation similar to the CIBR (see equation (7)), but with atmospheric pre-correction terms for the path radiances $L_{p,i}$:

$$T_m(PW) = \frac{L_m - L_{p,m}(PW)}{w_{r1}(L_{r1} - L_{p,r1}) + w_{r2}(L_{r2} - L_{p,r2})} \tag{4}$$

Note, however that $L_{p,m}$ is also a function of water vapor which can be expressed using a polynomial of second (or higher) order:

$$L_{p,m}(PW) = aPW^2 + bPW + c + L_{\text{adj,m}}, \tag{5}$$

where we neglect the adjacency path radiance $L_{\text{adj,m}}$ for now. In future work we plan to incorporate the adjacency effect in the retrieval over small dark targets and shadow regions where the adjacency effect dominates. The polynomial coefficients a, b and c are fitted to the total radiance over a zero ground reflectance computed by a radiative transfer code such as MODTRAN3 (Abreu et al., 1995) or 6S for the given observation geometry and assumed atmospheric conditions.

$$R_{APDA}(PW) \;=\; \frac{L_m - (aPW^2 + bPW + c)}{w_{r1}(L_{r1} - L_{p,r1}) + w_{r2}(L_{r2} - L_{p,r2})}. \tag{6}$$

The following iterative procedure can be used to compute the water vapor $PW(j,k)$ for pixel (j,k):

1. Use a radiative transfer code (6S or MODTRAN 3) to compute the path radiance $L_{p,m}$ for an average reflectance background (e.g. $\rho_{g,i} = 0.4$) as a function of water content and fit a polynomial (eq.(5)) to $L_{p,r1}$ and $L_{p,r2}$ for a zero reflectance background. Note that the path radiances $L_{p,r1}$ and $L_{p,r2}$ are assumed to be independent of PW.
2. Use a spectral radiative transfer code (6S or MODTRAN 3) to compute the total radiance over a zero reflectance background as a function of water vapor PW. Because the ratio $R_{APDA}(PW)$ decreases smoothly with increasing water vapor a spline interpolation is used to go from a given ratio to columnar water vapor.
3. Assume as a starting value an average water vapor $\overline{PW}_1$ for the whole scene.
4. Estimate $R_{APDA}(j,k)$ for each pixel (j,k) using equation (6) and use the cubic spline interpolation to get a second estimate $PW_2(j,k)$ for the columnar water vapor.
5. Substitute $PW_2(j,k)$ for PW the right side of equation (6) to get a better ratio $R_{APDA}(j,k)$.
6. Determine from the second ratio $R_{APDA}(j,k)$ a third water vapor amount $PW_3(j,k)$ using the cubic spline interpolation.
7. Repeat steps 5 and 6 a fixed number of times or until $|PW_i(j,k) - PW_{i-1}(j,k)| \leq 10^{-4}$.

We have compared this iterative technique with the optimum solution where we assume the water vapor is known exactly. The iterative solution performs within 0.5% of the optimal solution for the 6S generated data set (see section 4).

The continuum interpolated band ratio (CIBR) by contrast is defined as:

$$R_{CIBR} \;=\; \frac{L_m}{w_{r1}L_{r1} + w_{r2}L_{r2}} \tag{7}$$

If we assume that the ground reflectances $\rho_{g,i}$ are very low, equation (7) reduces to:

$$R_{CIBR}(\rho_{g,i} \approx 0.) \approx \frac{L_{p,m}(PW)}{w_{r1}L_{p,r1} + w_{r2}L_{p,r2}}. \quad (8)$$

Since $L_{p,r1}$ and $L_{p,r2}$ are constant, the CIBR is then proportional to the water vapor dependent path radiance $L_{p,m}(PW) = L_{h,m}[1 - T^*_m(PW)]$ which is no longer proportional to $T_m(PW)$. When the background reflectance is high, equation (7) reduces to:

$$R_{CIBR}(\rho_{g,i} \approx 1.) \approx Const\ T_m(PW). \quad (9)$$

Thus only for high background reflectances is the CIBR proportional to $T_m(PW)$ and thus can be used to retrieve water vapor.

3 Comparisons of the CIBR and APDA using a simple Radiative Transfer Model

To test equations (6) and (7) we computed irradiances, transmissions and path radiance (with MODTRAN3 using the DISORT option). The atmospheric state was mid-latitude summer, visibility of 23 km and the columnar water vapor was fixed at 2.4 g/cm^2. The target height was at 0.4 km, the Sun at 40 degrees with approximately 1 nm spacing. The ground reflectances $\rho_{g,1}$ and $\rho_{g,2}$ was changed from 0.05 to 1. in steps of 0.05 on both sides of the spectral range $(\lambda_{min(r1)}, \lambda_{max(r2)})$ which is defined as the minimum and maximum wavelengths of channels r1 and r2. The following formula is used to create the various reflectance background spectra:

$$\rho_g(\lambda) = \rho_{g,1} + \frac{\rho_{g,2} - \rho_{g,1}}{\lambda_{max(r2)} - \lambda_{min(r1)}}\lambda - \lambda_{min(r1)}. \quad (10)$$

The selected optimum AVIRIS bands (55, 62 and 68) for 1995 data have the following full-width-half-maximum $r1$: 0.869-0.879 μm, m: 0.936-0.946 μm and $r2$: 0.994-1.004 μm (see Schläpfer et al., 1996). From figure 2 it seems that the APDA is less sensitive to reflectance variations than the CIBR for both spectral cases.

If broader bands than AVIRIS are used in a multispectral sensor the simulation shows similar results. The selected bands are $r1$: 0.86-0.89 μm, m: 0.91-0.97 μm and $r2$: 0.99-1.04 μm. In figure 2 we show a scatterplot of all computed CIBR and APDA ratios as a function of the band-averaged reflectance in channel 2. Note the large range for the CIBR compared with the APDA techniques. Also the CIBR maps low reflectances ($\rho_{g,m} < 0.2$) to higher ratios, whereas the APDA maps all reflectances to an almost constant ratio. There is still a residual effect visible from reflectance slopes (markers forming lines with positive slopes) which could be corrected as well. The influence of reflectance slopes is similar for the CIBR and the APDA. The ratios or quasi water vapor transmittances for the AVIRIS case are much lower than for the multispectral case because the selected AVIRIS channel lies deep in an absorption feature. Note that we have not yet investigated how the APDA technique depends on atmospheric conditions (aerosol loading, etc), calibration errors and radiative transfer code uncertainties.

4 Comparisons of the CIBR and APDA for Variable Water Vapor and 562 Reflectance Spectra

We performed a simulation to test the behavior of CIBR and APDA techniques over spectrally varying backgrounds. Existing reflectance spectral data bases for 165 (Grove et al., 1992) and 25 (Kruse et al., 1992) minerals and the USGS spectral data base (only distinctive mineral names) (Clark et al., 1993) for many geologic

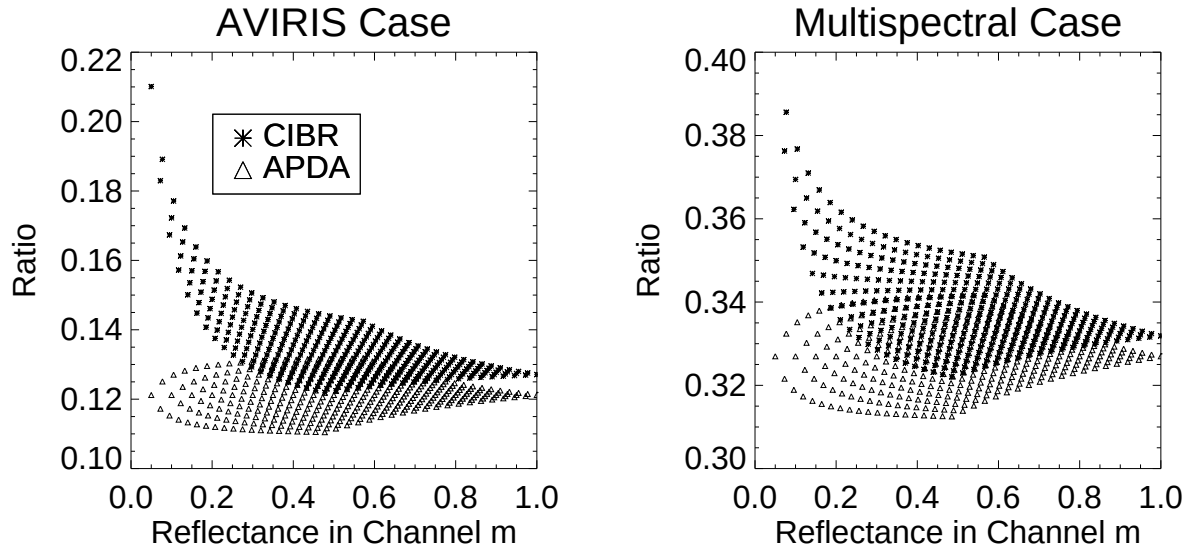

Figure 2: Water vapor ratios as a function of band-averaged ground reflectance of channel 2 for a 10 nm bandwidth instrument (AVIRIS) and a multispectral instrument using Duntley's model.

and vegetative surfaces were used as backgrounds. Because leaves contain significant amounts of water, a data base for 125 simulated leaf reflectance and transmittance spectra with variable leaf water content (0.0046 to 0.0405 cm) was created using the PROSPECT REDUX (Jacquemoud et al., 1995). The radiosity method was then used to compute canopy spectra of a 20-layer canopy with a total leaf area index (LAI) of 5. (Borel et al., 1990). In total 562 spectra were used vs. 379 in Borel and Schläpfer, 1996.

All 562 reflectance spectra were re-sampled at 2.5 nm spacings. The radiative transfer code 6S (Vermote et al., 1994) was used to compute the TOA radiance over the water vapor band centered on 940 nm. The water vapor amounts ranged from 0.05 to 5 g/cm^2 in 12 steps. The atmosphere had a constant visibility of 20 km with continental aerosols. The target height was set at sea level and the sensor located above the atmosphere. Only the data for common water vapor amounts $1 \leq PW \leq 4.g/cm^2$ was used in the following analysis. Figure 3 shows the RMS relative error in percent:

$$\varepsilon(PW_j) = 100\sqrt{\frac{1}{N}\sum_{i=1}^{N}[\frac{(PW_{j,true} - PW_{i,est})}{PW_{j,true}}]^2}$$

in water vapor for all N =562 reflectance spectra as a function of water vapor. The four different techniques are:

1. **CIBR**: Original CIBR equation (7).
2. **APDA**: Regular APDA equation (6) using a fixed water vapor amount of 2.5 g/cm^2 to compute the path radiance $L_{p,m}$.
3. **APDA (optimal)**: Equation (6) with computed water vapor dependent path radiance $L_{p,m}(PW)$.
4. **APDA (iterative)**: Equation (6) with the iterative scheme (5 iterations) described in section 2.

To compare the various water vapor retrieval techniques we defined a measure similar to a quasi signal to

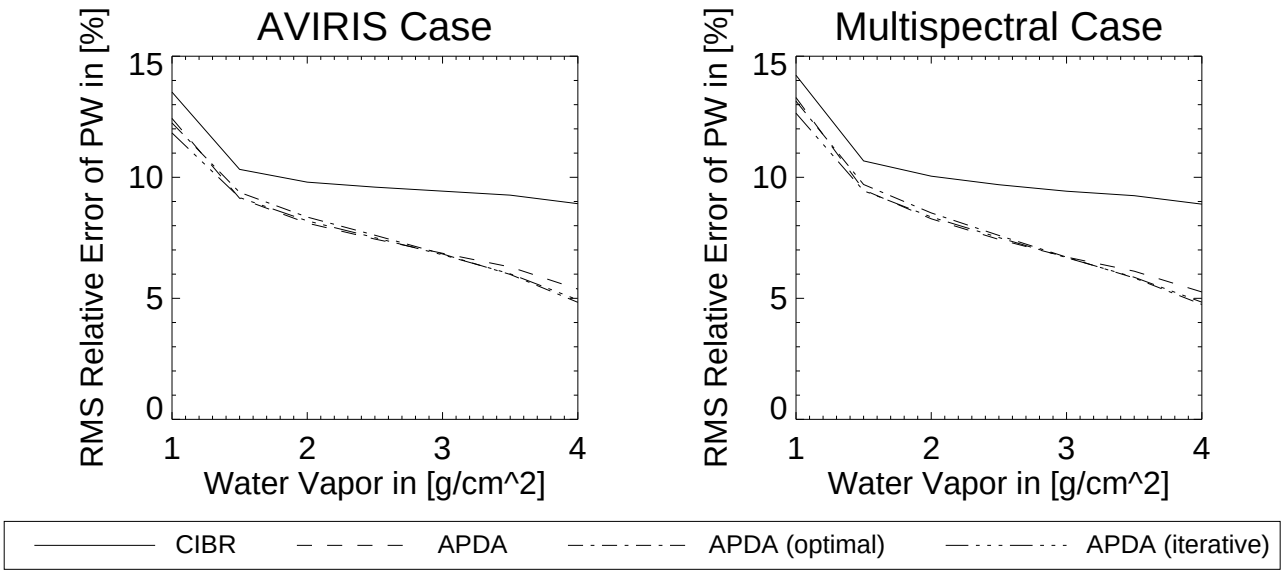

Figure 3: RMS relative error $\varepsilon(PW_j)$ in % water vapor for all 562 reflectance spectra as a function of water vapor for four different water vapor retrieval techniques.

noise ratio (SNR):

$$SNR(R_x(PW)) = \frac{\overline{R}_x(PW_{min})) - \overline{R}_x(PW_{max})}{\sigma(R_x(PW))}, \text{ where } x = \{\text{CIBR}, \text{APDA}, \text{APDA(optimal)}, \text{APDA(iterative)}\}, \quad (11)$$

where $PW_{min} = 1\ g/cm^2$ and $PW_{max} = 4\ g/cm^2$ are the minimum and maximum water vapor contents, $\overline{R_x(PW)}$ denotes the average over $R_x(PW)$, $\sigma(R_x(PW))$ denotes the standard deviation over $R_x(PW)$. Table 1 shows the minimum and maximum SNR for four retrieval techniques.

Table 1: SNR comparison

Case:	AVIRIS			Multispectral		
Retrieval Technique	Range of R	$\overline{\sigma(R)}$	$SNR_{min/max}$	Range of R	$\overline{\sigma(R)}$	$SNR_{min/max}$
CIBR	0.238	0.01768	12.3-13.9	0.233	0.01743	12.0-14.0
APDA	0.248	0.01277	13.6-24.2	0.243	0.01274	13.1-24.4
APDA (optimal)	0.240	0.01217	13.9-26.6	0.235	0.01216	13.5-26.6
APDA (iterative)	0.241	0.01233	13.9-26.3	0.237	0.01230	13.5-26.3

Next we compare the retrieval methods by setting thresholds at $\pm 5\%$ and $\pm 10\%$ RMS relative water vapor and counting the number of spectra which indicate how robust the retrievals are over many different backgrounds. Table 2 summarizes the results obtained for all 562 background spectra using the four above described techniques:

Table 2: Percentage of Materials above 5% and 10% RMS Relative Water Vapor Error

Retrieval Method	AVIRIS 5%	Multispectral 5%	AVIRIS 10%	Multispectral 10%
CIBR	30.6	32.6	13.9	15.6
APDA	21.9	22.4	6.4	5.7
APDA (optimal)	21.7	22.9	6.2	5.7
APDA (iterative)	21.0	21.7	6.2	5.7

Figure 4 shows a scatterplot of the relative water vapor errors over 562 backgrounds as a function of band-averaged ground reflectance. The result is that the CIBR has large water vapor errors for low ground reflectance and the regular and iterative APDA work better at low reflectance levels. The iterative APDA has a little more reflectance spectra above the ± 10% limit for the AVIRIS case than the multispectral approach, as is also evident from table 2. In both scatter plots the simulated vegetation spectra show up as two clustered sets of points along two lines between reflectances 0.55 and 0.66. The water vapor error is negative because vegetation has a water absorption feature which increases the apparent water vapor in the atmosphere. This feature could potentially be exploited to estimate canopy water content (Gao and Goetz, 1990b). The materials for which the iterative APDA had relative water vapor errors of more than ± 10% are listed below in Tables 3 and 4. Materials are listed in upper-case letters for the SIPS and lower case letters for the USGS. Double entries are listed only once.

Table 3: Percentage of Materials above 10% RMS Relative Water Vapor Error (AVIRIS Case)

Mineral	$\rho_{g,m}$	$\frac{\rho_{g,r2}-\rho_{g,r1}}{\rho_{g,r2}+\rho_{g,r1}}$	$R_{CIBR}(\rho_{g,r1},\rho_{g,m},\rho_{g,r2})$	$PW_{rel.err.,iter}$ in [%]
ANTHOPHYLLITE-IN-8A	0.559	0.013	-0.06	12.98
ANTLERITE-SO-11A	0.149	0.125	-0.08	18.22
AUGITE-IN-15A	0.079	0.345	-0.07	18.90
Axinite	0.173	-0.65	-0.29	67.28
Azurite	0.065	0.238	-0.08	20.52
BUDDINGTONITE-NHB2301	0.550	0.035	0.009	-10.2
Beryl	0.671	0.204	0.050	-10.4
Bronzite	0.134	0.262	-0.27	70.92
Chrysocolla	0.093	0.301	-0.07	18.06
Copiapite	0.332	0.211	-0.07	17.75
CUMMINGTONITE-IN-6A	0.128	-0.05	-0.10	19.66
DICKITE-PS-3A	0.055	-0.05	-0.09	15.07
ENSTATITE-IN-10B	0.295	0.159	-0.16	42.18
FAYALITE-NS-1A	0.089	-0.18	-0.09	14.95
H2O-Ice	0.769	-0.06	0.038	-11.1
HEMATITE-FE2602	0.231	0.236	-0.11	22.92
Hypersthene	0.415	0.121	-0.13	33.47
Jarosite	0.283	0.078	-0.09	19.51
Lepidocrosite	0.245	0.009	-0.08	16.45
Monazite	0.483	0.170	0.163	-35.5
Neodymium-Oxide	0.917	0.201	0.177	-40.7
MAGNESIOCHROMITE-O-8A	0.159	0.102	-0.05	10.81
MOLYBDENITE-S-11A	0.254	0.191	0.054	-10.5
NONTRONITE-PS-6D	0.339	0.039	-0.05	10.13
Praseodymium-Oxide	0.056	0.266	-0.07	16.93
TOURMALINE-DRAVITE-S-CS-1A	0.083	-0.10	0.059	-15.3
TREMOLITE-AMT3001	0.701	-0.09	0.006	-12.1
Samarium-Oxide	0.797	-0.03	-0.11	22.08
Siderite	0.113	-0.20	-0.08	13.02
Tephroite	0.138	-0.07	-0.07	12.55
Vesuvianite	0.628	0.014	-0.04	10.04

Table 4 : Percentage of Materials above 10% RMS Relative Water Vapor Error (Multispectral Case)

Mineral	$\rho_{g,m}$	$\frac{\rho_{g,r2}-\rho_{g,r1}}{\rho_{g,r2}+\rho_{g,r1}}$	$R_{CIBR}(\rho_{g,r1},\rho_{g,m},\rho_{g,r2})$	$PW_{rel.err.,iter}$ in [%]
ANTHOPHYLLITE-IN-8A	0.559	0.013	-0.06	12.64
ANTLERITE-SO-11A	0.149	0.125	-0.10	14.22
Augite	0.290	-0.19	-0.02	10.63
Axinite	0.173	-0.65	-0.22	86.29
Azurite	0.065	0.238	-0.11	13.26
Beryl	0.671	0.204	0.020	-16.8
Bronzite	0.134	0.262	-0.29	62.32
BUDDINGTONITE-NHB2301	0.550	0.035	0.004	-11.2
Copiapite	0.332	0.211	-0.09	10.74
Cuprite	0.157	0.115	0.021	-12.3
CUMMINGTONITE-IN-6A	0.128	-0.05	-0.09	21.56
DICKITE-PS-3A	0.055	-0.05	-0.08	16.73
ENSTATITE-IN-10B	0.295	0.159	-0.18	36.64
FAYALITE-NS-1A	0.089	-0.18	-0.07	20.61
HEMATITE-FE2602	0.231	0.236	-0.14	15.02
Hypersthene	0.415	0.121	-0.14	29.28
Jarosite	0.283	0.078	-0.10	16.97
Lepidocrosite	0.245	0.009	-0.08	16.17
Monazite	0.483	0.170	0.135	-41.4
MOLYBDENITE-S-11A	0.254	0.191	0.025	-16.3
Neodymium-Oxide	0.917	0.201	0.144	-48.2
Samarium-Oxide	0.797	-0.03	-0.11	23.24
Siderite	0.113	-0.20	-0.05	19.34
Sphalerite	0.466	0.169	0.003	-10.6
SIDERITE-COS2002	0.204	-0.24	-0.05	15.01
TOURMALINE-DRAVITE-S-CS-1A	0.083	-0.10	0.075	-12.3
TRIPHYLITE-P-4A	0.440	-0.30	-0.02	18.89
Tephroite	0.138	-0.07	-0.06	14.93

A spectrum was classified as 'dark' if the average reflectance in channel $\rho_{g,m}$ was below 0.1. A spectrum was considered 'sloped' if the absolute of the normalized difference:

$$R_{slope} = \frac{|\overline{\rho_{g,r1}} - \overline{\rho_{g,r2}}|}{\overline{\rho_{g,r1}} + \overline{\rho_{g,r2}}}$$

between the channel averaged reflectances of channels $r1$ and $r2$ exceeded 0.05. A spectrum was considered 'non-linear' if the ratio:

$$R_{non-linear} = \frac{\overline{\rho_{g,m}}}{w_{r1}\overline{\rho_{g,r1}} + w_{r2}\overline{\rho_{g,r2}}}$$

was less than 0.95 or greater than 1.05. From the tables 3 and 4 we readily see that the nonlinear measure correlates well with the water vapor error.

5 Conclusions

An efficient technique to determine the amount of columnar water vapor has been derived from a modified radiative transfer equation. The technique seems to work much better than the current CIBR techniques which neglect the effects of path radiance. We show how the CIBR and APDA behave over dark, bright and spectrally

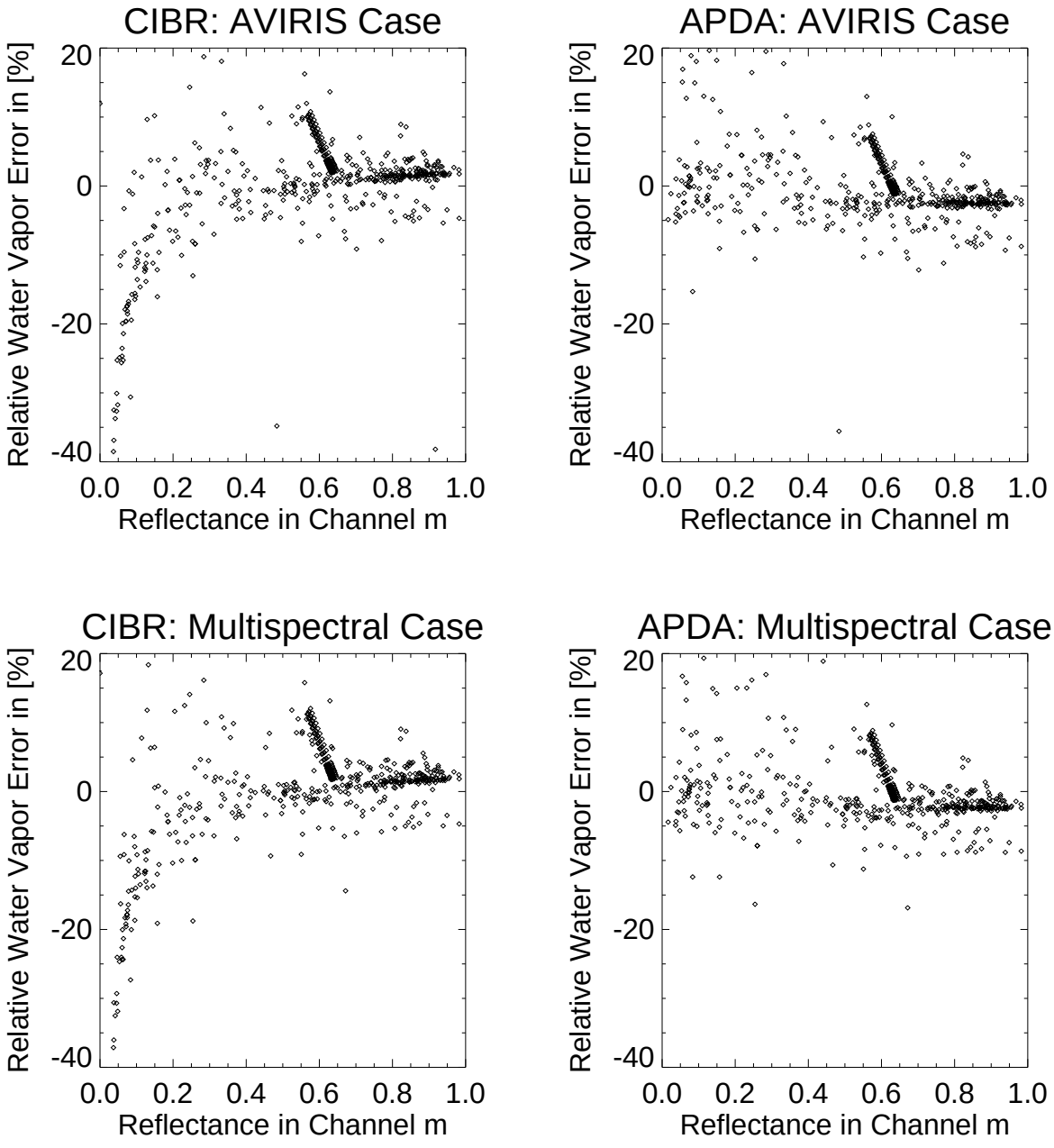

Figure 4: Relative water vapor errors over 562 backgrounds as a function of band-averaged ground reflectance for a 10 nm bandwidth instrument (AVIRIS) and a multispectral instrument. Note the points that line up near 0.6 reflectance are from canopy spectra.

variable backgrounds. A large number of measured mineral spectra and measured/simulated vegetation spectra were used and the relative water vapor error lies within $\pm 5\%$ for most reflectance spectra. We think this accuracy is sufficient for current applications since sensor calibration and modeling errors are estimated to have similar relative errors. A challenge remains to determine water vapor over dark surfaces such as water since the path radiance is now the only quantity containing information about the water vapor. More work is also needed to retrieve water vapor in rough terrain. The presented techniques may also be useful to retrieve other gases such as O_2 and in conjunction to aerosol retrievals.

6 Acknowledgments

This work has been funded by NASA HQ's Remote Sensing Science Program and the Department of Energy. The principal author acknowledges many fruitful technical discussions with and work done by Daniel Schläpfer (RSL, Univ. of Zürich, Switzerland) and by Veronique Carrére (ISPRA, Italy). James Theiler (LANL) reviewed the paper very carefully.

7 References

Abreu L.W., Chetwynd J.H, Anderson G.P. and Kimball L.M., 1995, MODTRAN 3 Scientific Report. Draft Preprint, Geophysics Laboratory, Air Force Command, US Air Force, Hanscom AFB, MA, USA.

Borel C.C. and Gerstl S.A.W., 1994, Non-linear Spectral Mixing Models for Vegetative and Soil Surfaces, Remote Sens. of the Environment, 47, pp 403-416.

Borel, C.C, and Schläpfer, D., 1996, Atmospheric Pre-Corrected Differential Absorption Techniques To Retrieve Columnar Water Vapor: Theory, Proceedings of the 6th JPL Airborne Earth Science Workshop, JPL, Pasadena.

Bruegge C.J., Conel J.E., Margolis J.S., Green R.O., Toon G., Carrére V., Holm R.G. and Hoover G., 1990, In-situ Atmospheric Water-Vapor Retrieval in Support of AVIRIS Validation., SPIE Vol. 1298 Imaging Spectroscopy of the Terrestrial Environment, pp 150 - 163.

Carrére V. and Conel J. E., 1993, Recovery of Atmospheric Water Vapor Total Column Abundance from Imaging Spectrometer Data around 940 nm - Sensitivity Analysis and Application to Airborne Visible/ Infrared Imaging Spectrometer (AVIRIS) Data. Remote Sensing of Environment, Nr. 44 , pp 179 - 204.

Clark R.N., Swayze G.A., Gallagher A.J., King T.V.V. and Calvin W.M., 1993, U.S. Geological Survey, Open File Report 93-592 or anonymous FTP: speclab.cr.usgs.gov or e-mail to rclark@speclab.cr.usgs.gov.

Frouin R., Deschamps P.-Y and Lecomte P., 1990, Determination from Space of Atmospheric Total Water Vapor Amounts by Differential Absorption Near 940 nm: Theory and Airborne Verification. Journal of Applied Meteorology, Vol. 29, American Meteorological Society, pp 448 - 459.

Gao B.-C. and Goetz A.F.H., 1990a, Determination of Total Column Water Vapor in the Atmosphere At High Spatial Resolution from AVIRIS Data Using Spectral Curve Fitting and Band Ratioing Techniques, SPIE Vol.

1298, Imaging Spectroscopy of the Terrestrial Environment, pp 138 - 149.

Gao B.-C. and Goetz A.F.H., 1990b, Column Atmospheric Water Vapor and Vegetation Liquid Water Retrievals from Airborne Imaging Spectrometer Data, Journal of Geophysical Research, Vol. 95, No. D4, pp 3549 - 3564.

Green, R.O., Carrére V. and Conel J.E., 1989, Measurement of Atmospheric Water Vapor Using the Airborne Visible/Infrared Imaging Spectrometer, Am. Soc. Photogram. and Remote Sensing Proc., Workshop Image Processing, Sparkes, Nevada, 23-26 May.

Grove C.I., Hook S.J. and Paylor E.D., 1992, Spectral Reflectance of Minerals 0.4 to 2.5 Micrometers, JPL Publication 92-2.

Jacquemoud S., Ustin S.L., Verdebout J., Schmuck G., Andreoli G. and Hosgood B., 1995, PROSPECT REDUX, Proceedings AVIRIS Workshop, Pasadena, January.

Kruse F.A., 1992, unpublished data.

Middleton, W.E.K., 1952, "Vision Through the Atmosphere," University of Toronto Press.

Schläpfer, D., Borel, C.C., Keller, J., and Itten, K., 1996, Atmospheric Pre-Corrected Differential Absorption Techniques to Retrieve Columnar Water Vapor: Application to AVIRIS 91/95 Data, Proceedings AVIRIS Workshop, Pasadena (CA).

Vermote E., Tanré D., Deuzé J.L., Herman M. and Morcette J.J., 1994, Second Simulation of the Satellite Signal in the Solar Spectrum. - 6S User Guide Version 0, NASA-Goddard Space Flight Center, Greenbelt, USA, p 182.